Attribute-filtering and knowledge extraction for vessel segmentation

Benoît Caldairou, Nicolas Passat, Benoît Naegel

Attribute-filtering and knowledge extraction for vessel segmentation

Benoît Caldairou[a,b], Nicolas Passat[a], Benoît Naegel[c]

(a) Université de Strasbourg, LSIIT, UMR CNRS 7005, France
(b) Université de Strasbourg, LINC, UMR CNRS 7191, France
(c) Université Nancy 1, LORIA, UMR CNRS 7503, France
e-mail: {caldairou, passat}@unistra.fr, benoit.naegel@loria.fr

Abstract. Attribute-filtering, relying on the notion of component-tree, enables to process grey-level images by taking into account high-level *a priori* knowledge. Based on these notions, a method is proposed for automatic segmentation of vascular structures from phase-contrast magnetic resonance angiography. Experiments performed on 16 images and validations by comparison to results obtained by two human experts emphasise the relevance of the method.

Key words: vessel segmentation, mathematical morphology, component-trees, magnetic resonance angiography.

1 Introduction

For a long time, mathematical morphology has been involved in the design of vessel segmentation methods[1] by only considering low-level operators (see, *e.g.*, [7, 5]). The ability of high-level operators to be efficiently considered for medical image processing has been pointed out in recent works [6], especially in the context of vessel segmentation [12, 16, 1]. The usefulness of such mathematical morphology operators –including those based on component-trees– is justified by their intrinsic capacity to model morphological information, and then to enable anatomical knowledge-guided approaches.

The notion of *component-tree* [15, 9, 4] associates to a grey-level image a descriptive data structure induced by the inclusion relation between the binary components obtained at the successive level sets of the image. In particular, it has led to the development of morphological operators [2, 15].

Thanks to efforts devoted to its efficient computation [2, 15, 13], component-trees have been considered for the design of various kinds of grey-level image processing methods, including image filtering and segmentation [9, 19, 18], some of them being devoted to the analysis of (bio)medical images: CT/MR angiography [21], confocal microscopy [14], dermatological data [11]. Some of these methods are automatic, can filter complex objects in 3-D images [21, 14], or take into account complex anatomical knowledge [11]. However none of them fuses all these virtues. The challenges to be faced towards the development of efficient medical image segmentation methods

[1] A whole state of the art on vessel segmentation is beyond the scope of this article. The reader may refer to [10] for a recent survey.

based on component-trees then consists in simultaneously dealing with *automation* and *complexity* requirements.

Based on advances related to the use of component-trees in this difficult context [17, 3], a method has been developed for the segmentation of phase-contrast magnetic resonance angiography (PC-MRA). Indeed, such data –non invasive, non-irradiant, and then harmless for the patients– are often considered in clinical routine, but generally not in the literature devoted to vessel segmentation. The low SNR and resolution of PC-MRAs however justify the use of segmentation methods in order to simplify their analysis.

The remainder of this article is organised as follows. Section 2 provides background notions on component-trees. Section 3 describes the proposed vessel segmentation method. Section 4 provides experimental results and validations. Section 5 summarises the contributions, and describes further works.

2 Component-trees

Let $I : E \to V$ (we also note $I \in V^E$) be a discrete grey-level image (with $E \subset \mathbb{Z}^n$ and $V = [\![a, b]\!] \subset \mathbb{Z}$), as illustrated in Fig. 1(a).

Let $X \subseteq E$ be a binary image. The connected components of X are the equivalence classes of X w.r.t. a chosen adjacency relation. The set of the connected components of X is noted $C[X]$.

Let $v \in V$. We set $\mathcal{P}(E) = \{X \subseteq E\}$. Let $X_v : V^E \to \mathcal{P}(E)$ be the thresholding function defined by $X_v(I) = \{x \in E \mid v \leq I(x)\}$ for all $I : E \to V$ (see Fig. 1(b–f)).

Let $v \in V$ and $X \subseteq E$. We define the cylinder function $C_{X,v} : E \to V$ by $C_{X,v}(x) = v$ if $x \in X$ and a otherwise. A discrete image $I \in V^E$ can then be expressed as $I = \bigvee_{v \in V} \bigvee_{X \in C[X_v(I)]} C_{X,v}$, where $\bigvee$ is the pointwise supremum for the sets of functions.

Let $\mathcal{K} = \bigcup_{v \in V} C[X_v(I)]$. The inclusion relation $\subseteq$ is a partial order on $\mathcal{K}$. Let $v_1 \leq v_2 \in V$. Let $B_1, B_2 \subseteq E$ be the binary images defined by $B_k = X_{v_k}(I)$ for $k \in \{1, 2\}$. Let $C_2 \in C[B_2]$ be a connected component of B_2. Then, there exists a (unique) connected component $C_1 \in C[B_1]$ of B_1 such that $C_2 \subseteq C_1$ (see Fig. 1(b–f)). In particular, we necessarily have $B_2 \subseteq B_1$.

Based on these properties, is can be easily deduced that the Hasse diagram of the partially ordered set $(\mathcal{K}, \subseteq)$ is a tree (*i.e.*, a connected acyclic graph), the root of which is its supremum $X_a(I) = E$. This tree is called the *component-tree of* I (see Fig. 1(g)).

Definition 1 (Component-tree). *Let $I \in V^E$ be a grey-level image. The* component-tree *of I is the rooted tree $(\mathcal{K}, L, R)$ such that: $\mathcal{K} = \bigcup_{v \in V} C[X_v(I)]$ (namely the* nodes*); $R = \sup(\mathcal{K}, \subseteq) = X_a(I)$ (namely the* root*); L (namely the set of* edges*) is composed of all pairs $(X, Y) \in \mathcal{K} \times \mathcal{K}$ verifying (i) $Y \subset X$ and (ii) $\forall Z \in \mathcal{K}, Y \subseteq Z \subset X \Rightarrow Y = Z$.*

In Fig. 1(g), $\mathcal{K}$ is the set of white rectangles, R is the one located at the highest level, and L is visualised by the set of black lines (linking the elements of each pair).

Component-trees enable the storage, at each node, of *attributes*, *i.e.*, elements of information related to the binary connected components associated to the nodes. For instance, in Fig. 1(g), the size of the connected component has been added at each corresponding node. In this (simple) example, the considered attribute is a single numerical

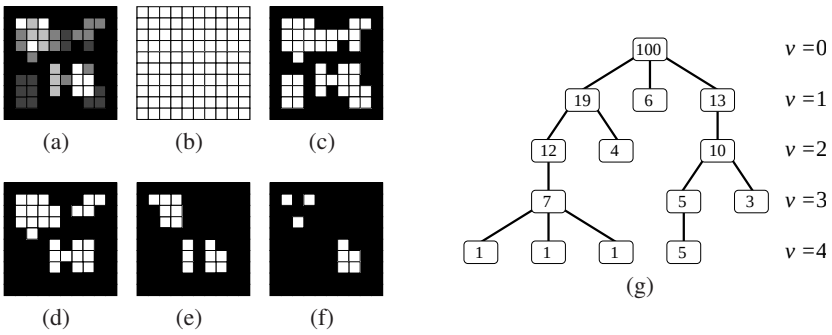

Fig. 1. (a) A grey-level image $I : [\![0,9]\!]^2 \to [\![0,4]\!]$. (b–f) Threshold images $X_v(I)$ (white points) for v varying from 0 (b) to 4 (f). (g) The component-tree of I. Its levels correspond to increasing thresholding values v. The root ($v = 0$) corresponds to the support ($E = [\![0,9]\!]^2$) of the image.

value. It is however possible to consider any kinds of –quantitative or qualitative– attributes, provided they can be conveniently modelled. It is also possible to store several elements of information, no longer leading to scalar attributes but to vectorial ones [17].

3 Segmentation method

The proposed method (summarised in the flowchart of Fig. 2) consists in (*i*) determining the characteristic properties of the structures of interest (vessels) thanks to a supervised learning process (Subsection 3.1), and (*ii*) using this knowledge to automatically process images *via* their component-tree (Subsection 3.2).

3.1 Learning process

This first step (see Fig. 2(a)) enables to extract from one (or possibly several) ground-truth data (*i.e.*, correctly segmented images) a set of characteristic parameters chosen from a given set of criteria.

The learning step takes as input (*i*) a ground-truth image $I_g \in V^E$, (*ii*) its segmentation $B_g \subset E$, and (*iii*) a function $A : \mathcal{P}(E) \to \Omega$, associating to each possible node of the component-tree of I_g, a feature vector in the parameter space Ω induced by a chosen set of criteria. It provides as output a subset $\omega \subset \Omega$ of the parameter space, characterising the nodes of the component-tree of I_g which enable to fit at best the segmentation B_g.

Let $(\mathcal{K}, L, R)$ be the component-tree of I_g. Let $\mathcal{S} = \{\bigcup_{X \in C} X\}_{C \subseteq \mathcal{K}}$ be the set of all the binary images which can be generated from the set of nodes $\mathcal{K}$. We need to determine the "best" binary image which may be computed from $\mathcal{K}$ w.r.t. B_g. This requires to define a distance d on $\mathcal{P}(E)$ enabling to compare B_g and the binary images of $\mathcal{S}$. The best binary image $\widehat{B}$ can be set as $\widehat{B} = \arg\min_{B \in \mathcal{S}}\{d(B, B_g)\}$. We define such a distance d by $d(B, B_g) = \alpha.|B \setminus B_g| + (1 - \alpha).|B_g \setminus B|$, with $\alpha \in [0, 1]$. It aims at finding a best compromise (parametrised by α) between the amount of false positives/negatives of B w.r.t. B_g.

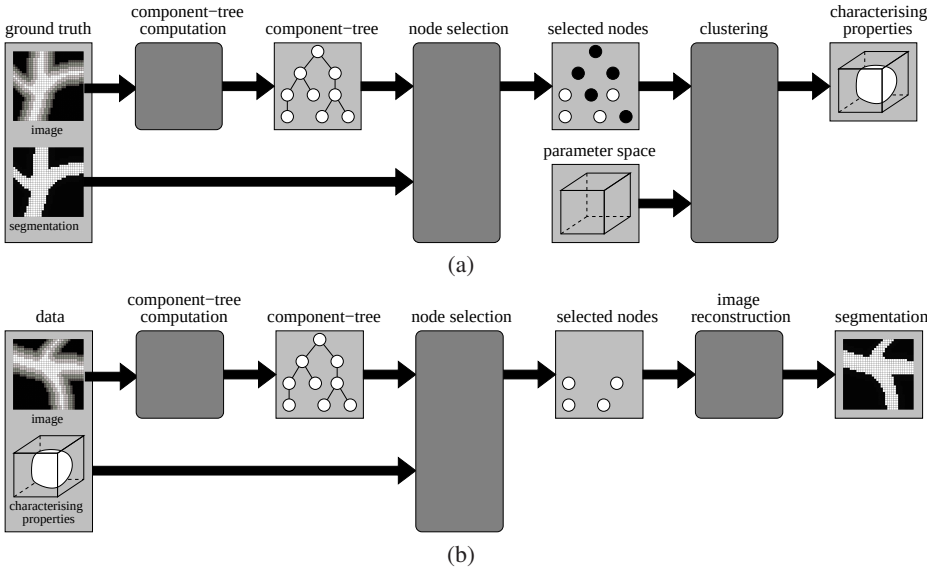

Fig. 2. Summary of the method (dark grey: processes; light grey: data). (a) Learning process. (b) Segmentation process.

Based on these definitions, a minimal set $\widehat{B}$ can be extracted from $\mathcal{S}$ (in linear time $O(|\mathcal{K}|)$). Then, an adequate set of nodes $\widehat{K} \subseteq \mathcal{K}$ associated to $\widehat{B}$ (*i.e.*, such that $\bigcup_{X \in \widehat{K}} X = \widehat{B}$) has to be determined. Let $\widehat{C} = \{X \in \mathcal{K} \mid X \subseteq \widehat{B}\} \subseteq \mathcal{K}$ (note that the nodes of $\widehat{C}$ generate a set of subtrees of the component-tree $(\mathcal{K}, L, R)$ of I_g). The set $\widehat{B}$ can be generated by any set of nodes $\widehat{K} \subseteq \widehat{C}$ verifying $\bigcup_{X \in \widehat{K}} X = \bigcup_{X \in \widehat{C}} X = \widehat{B}$. Two main strategies can be considered: by setting $\widehat{K}^+ = \widehat{C}$, any node included in $\widehat{B}$ is considered as a useful binary connected component, while by setting $\widehat{K}^- = \{X \in \widehat{C} \mid \forall Y \in \widehat{C}, X \not\subset Y\}$, only the roots of the subtrees induced by $\widehat{C}$ are considered as useful. The first (resp. second) strategy is the one considering the largest (resp. smallest) possible set of nodes/connected components among $\widehat{C}$.

Once a set of nodes $\widehat{K}$ has been defined, the determination of the subset of characterising knowledge $\omega \subset \Omega$ has to be performed. The determination of ω can be expressed as a clustering problem consisting in partitioning Ω into two classes thanks to the samples $A(\widehat{K}) = \{A(N)\}_{N \in \widehat{K}}$ (corresponding to the attributes of the structures of interest) and $A(\mathcal{K} \setminus \widehat{C}) = \{A(N)\}_{N \in \mathcal{K} \setminus \widehat{C}}$. This process can, for instance, be carried out by usual classification tools, such as the Support Vector Machine (SVM) [20].

3.2 Segmentation process

This second step (see Fig. 2(b)) enables to segment the structures of interest from an image, based on the characterising properties modelled by the set of knowledge $\omega \subset \Omega$.

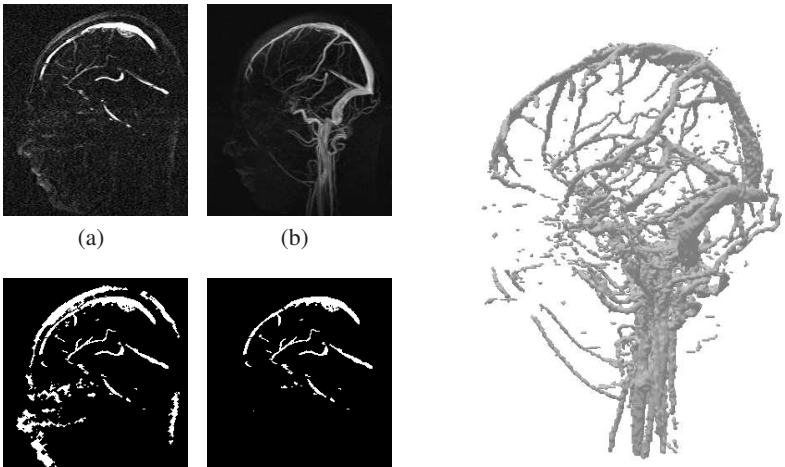

Fig. 3. (a,b) Cerebral PC-MRA (this image has been used as ground-truth): (a) sagittal slice, (b) maximum intensity projection. (c–e) Ground-truth segmentation of (a): vessels and artifacts ($B_v \cup B_a$) (c); vessels only (B_v) (d), 3-D visualisation of vessels (B_v) (e).

The segmentation step takes as input an image $I \in V^E$ and a subset $\omega \subset \Omega$ characterising the structures to be segmented in I. It provides as output a segmentation $B \subseteq E$ of these structures of interest.

Let $(\mathcal{K}, L, R)$ be the component-tree of I. We define $\mathcal{K}_f = \{N \in \mathcal{K} \mid A(N) \in \omega\}$. The set $\mathcal{K}_f$ is composed of the nodes which satisfy the characterising properties modelled by ω, and are then considered as the parts of the image to be preserved by the segmentation process. We can finally reconstruct the segmentation result as $B = \bigcup_{N \in \mathcal{K}_f} N$.

4 Experiments and results

4.1 PC-MRA segmentation

The proposed methodology has been considered for the segmentation of cerebral PC-MRAs. Such images (see Fig. 3(a,b)) are composed of three kinds of semantic elements: low-intensity background, high-intensity artifacts and high-intensity vascular signal.

Input/output The method processes PC-MRA images $I \in V^E$ (with $E = [\![0, 255]\!]^3$ and $V \subset \mathbb{N}$). The learning step requires a ground-truth image $I_g \in V^E$ (Fig. 3(a,b)), and its segmentation $B_v \subset E$ (vessels) and $B_a \subset E$ (artifacts) (Fig. 3(c–e)). The segmentation step provides as output a fuzzy segmentation $S \in [0, 1]^E$ of the vessels visualised in I.

Multiscale approach In order to deal with the complexity of the structures of interest, the segmentation method can be applied in a multiscale fashion. The image is then processed as a collection of subimages obtained from an octree decomposition, thus enabling to "break" complex structures into smaller –and easier to characterise– ones. In order to improve the behaviour of the method at the border of these subimages, it can be convenient to consider two shifted octree decompositions of the image. In such a context, if the octrees have d levels, any point $x \in E$ of the image belongs to $2d$ subimages, the sizes of which vary from 256^3 to $(256/2^{d-1})^3$. (Note that this octree decomposition also has to be considered in the learning step, resulting in a distinct set ω for each one of the d subimage sizes.) This value $2d$ can be seen as a redundancy factor of the multiscale segmentation method. In our case, the value d has been set to 4.

By opposition to the initially proposed strategy, the variant proposed here does not provide a binary result $B \subseteq E$. Indeed, overlaps induced by multiscale and redundancy may lead to ambiguous results for any point $x \in E$. A grey-scale segmentation $S \in \mathbb{R}^E$ can however be obtained by setting $S(x) = s(x)/2d$, where $s(x) \in \mathbb{N}$ is the number of nodes which contain x (among the component-trees induced by the $2d$ subimages where x appears) and which have been classified as being vascular. This segmentation S (which can be assimilated to a fuzzy segmentation, although not normalised) provides, for each point $x \in E$, a value which can be seen as a "vesselness" score.

Learning step: Presegmentation In order to perform the learning step, it is first required to choose the best segmentation results w.r.t. the ground-truth segmentations B_v and B_a and the distance d. Several results have then been computed, for various values of α (which determines the authorised ratio between false positives/negatives) sampled in $[0, 1]$. The most satisfying sets $\widehat{B_v}$ and $\widehat{B_a}$ have then been chosen by a human expert, based on a visual analysis. (Note that in the current experiments, the corresponding value of α was 0.9 for B_v and 0.4 for B_a.) The associated sets of nodes $\widehat{K_v}$ and $\widehat{K_a}$ have been defined as $\widehat{K_v^-}$ and $\widehat{K_a^-}$, respectively. Indeed, it has been chosen to give a higher importance to the shape of the structures than to their grey-level profile (since only the roots of the component-trees induced by the best segmentation results are then considered, see Subsection 3.1).

Learning step: Parameter estimation In order to determine a set ω characterising the high-intensity vascular signal from the background noise and the high-intensity artifacts, a three class SVM classification has been applied on the component-trees of I_g, using the parameter space Ω induced by the following attributes: moment of inertia, flatness (computed from the eigenvalues of the inertia matrix of I), intensity, size, volume (related to the grey-level profile of the image at the node), contrast (distance between the node and the closest leaf in the component-tree), distance to the head (computed thanks to the morphological image associated to I). Among these attributes, some "simple" ones (*e.g.* intensity, size) are considered in order to enable the classification between the background noise and the high intensity structures (vessels and artifacts), while some more sophisticated ones (*e.g.* moment of inertia, flatness) are assumed to enable the discrimination between vessels and artifacts, since they are dedicated to shape characterisation [8].

Segmentation step The obtained set $\omega \subset \Omega$ has then been used to determine the desired set of nodes $\mathcal{K}_s(k,l) \subseteq \mathcal{K}$ from each set of component-trees of I, for each octree decomposition $k = 1, 2$, and at each level $l = 1$ to d. From these sets of nodes, it has been possible to build a segmented grey-level image $I_s : E \to \mathbb{R}$ defined by

$$I_s(x) = \frac{1}{2d} \sum_{k=1}^{2} \sum_{l=1}^{d} |\mathcal{K}_s(k,l) \cap \{X \mid x \in X\}| \tag{1}$$

In particular, $I_s(x) = 0$ (resp. $\neq 0$, resp. $\gg 1$) means that x never matches a vessel (resp. matches at least once a vessel, resp. often matches a vessel) in the segmentation result.

4.2 Results

Technical details The method has been applied on a database composed of 17 PC-MRAs (Philips Gyroscan NT/INTERA 1.0 T, TR = 10 ms, TE = 6.4 ms), of millimetric resolution (see Fig. 3(a,b)). One image has been considered for the learning step (I_g) while the other 16 ones have been considered for quantitative validations.

With a standard PC (Intel Quad Core i7 860, 4GB RAM), the average computation time for the method is 3 min/image for the learning step (which only requires to be carried out once), and 4 min/image for the segmentation step.

Validations The 16 MRAs have also been interactively segmented by two human experts. These results $S_e^1, S_e^2 \subset E$ are generally slightly different. Indeed, the mean of the maximal sensitivity (resp. minimal sensitivity) between S_e^1 and S_e^2 is 87.2% (resp. 68.3%). This tends to mean that the accurate segmentation of such images (presenting a very low SNR) is a complex and error-prone task, even for experts. Based on this uncertainty, we set $V = S_e^1 \cap S_e^2$, $\overline{V} = E \setminus (S_e^1 \cup S_e^2)$, and $V_? = (S_e^1 \setminus S_e^2) \cup (S_e^2 \setminus S_e^1)$, assumed to be the vascular, non-vascular, and ambiguous areas, according to these ground-truths.

For each MRA, let $S \subset E$ be a visually satisfactory segmentation obtained from I_s (by interactive thresholding of I_s, which requires only a few seconds; we provide in Tab. 1 the threshold value λ such that $S = I_s(\lambda)$). Let TP $= |V \cap S|$, AP $= |V_? \cap S|$, FP $= |\overline{V} \cap S|$, the true, ambiguous and false positives of S w.r.t. the ground-truth, respectively. Let TN $= |\overline{V} \setminus S|$, AN $= |V_? \setminus S|$, FN $= |V \setminus S|$, the true, ambiguous and false negatives of S w.r.t. the ground-truth, respectively. In the standard case (*i.e.*, when $V_? = \emptyset$), the formulae for sensitivity (Sen) and specificity (Spe) are given by Sen $=$ TP/(TP + FP) and Spe $=$ TP/(TP + FN). Here, since $V_? \neq \emptyset$, we can only compute intervals $[\text{Sen}^-, \text{Sen}^+], [\text{Spe}^-, \text{Spe}^+] \subseteq [0,1]$ providing the potential sensitivity and specificity values induced by the uncertainty on the ground-truth. The bounds of these intervals are straightforwardly given by

$$\text{Spe}^+ = (\text{TP} + \text{AP})/(\text{TP} + \text{FN} + \text{AP}) \tag{2}$$

$$\text{Spe}^- = \text{TP}/(\text{TP} + \text{FN} + \text{AN}) \tag{3}$$

$$\text{Sen}^+ = (\text{TP} + \text{AP})/(\text{TP} + \text{FP} + \text{AP}) \tag{4}$$

$$\text{Sen}^- = \text{TP}/(\text{TP} + \text{FP} + \text{AP}) \tag{5}$$

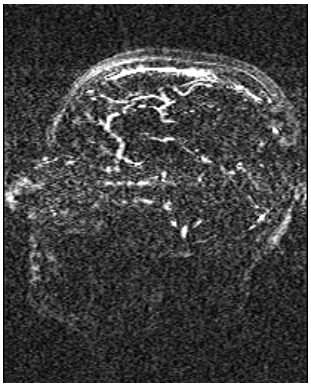

(a)

(b)

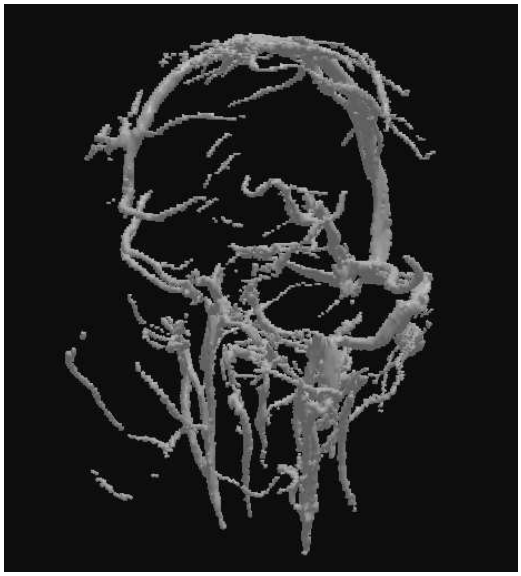

(c)

Fig. 4. (a) MRA (I) and (b) its grey-level segmentation (I_S) viewed as a MIP (line 15 in Table 1). (c) Binary segmentation (S) viewed as a 3-D object (line 11 in Table 1, $\lambda = 40.3$).

Table 1. Quantitative analysis of the segmentation results (see text).

	λ	Spe (%)	Sen (%)	$d(S,V)$
1	100	[49.3, 79.8]	[77.6, 85.0]	2.8 ± 7.7
2	50	[51.7, 77.5]	[80.4, 85.5]	1.5 ± 5.2
3	120	[47.7, 66.6]	[79.3, 77.0]	4.0 ± 10.8
4	80	[46.8, 66.0]	[88.5, 87.3]	1.8 ± 5.0
5	80	[33.3, 64.1]	[83.3, 87.4]	2.3 ± 5.9
6	100	[34.6, 58.9]	[86.4, 89.0]	3.6 ± 11.2
7	80	[28.5, 46.6]	[71.2, 75.7]	2.1 ± 4.2
8	80	[43.3, 65.2]	[68.4, 74.5]	3.5 ± 8.1
9	80	[39.9, 57.7]	[75.8, 77.3]	2.0 ± 4.3
10	150	[38.8, 62.9]	[63.7, 68.7]	3.8 ± 7.6
11	50	[48.7, 74.8]	[80.6, 87.9]	1.7 ± 5.1
12	50	[43.2, 68.9]	[83.1, 89.5]	1.6 ± 4.9
13	80	[33.9, 65.2]	[62.9, 73.1]	4.8 ± 10.3
14	100	[35.7, 63.4]	[71.2, 74.3]	2.5 ± 6.5
15	150	[36.6, 65.2]	[67.1, 77.8]	2.7 ± 6.2
16	100	[36.0, 65.4]	[62.1, 66.7]	5.5 ± 11.5

From a quantitative point of view (see Tab. 1 for intervals $[Sen^-, Sen^+]$, $[Spe^-, Spe^+]$ and mean point-to-set distance between S and V, in mm), the measures can appear as low. If this can be partially explained by possible segmentation errors (the main errors generally result from the loss of the smallest vessels, composed of small connected components less accurately modelled by the considered attributes), it also results from the quality of the ground-truths (which contain several errors, as aforementioned). Moreover, the proposed segmentations are grey-level ones (see Fig. 4(a,b)), which can be thresholded to favour either sensitivity or specificity. The binary segmentation obtained by such a thresholding (see Fig. 4(c)) also emphasises the ability of the method to provide qualitatively satisfactory results. Finally, one has to note that the experts provided results in approximately one hour by using interactive tools, *vs.* a few minutes for the method.

5 Conclusion

Based on the notion of component-tree, a method has been proposed for the segmentation of angiographic data. It takes advantage of *a priori* knowledge, thanks to a learning process enabling to define characteristic properties of vessels. This knowledge is, in particular, embeddable in the component-tree structure of the images to be processed.

The validations performed on phase-contrast images tend to emphasise the relevance of the proposed methodology, in particular by comparison to segmentations performed by human experts (from both qualitative and time-consumption points of view). It has to be noticed that vessel segmentation method, although being fast and automated, however still presents a few weaknesses, especially in the detection of small vessels.

In order to improve its robustness, further works will focus on the following points: (*i*) automatic choice of the pertinent parameters enabling to determine the Ω space (enabling to initially consider a larger set of potential parameters), (*ii*) incremental improvement of the learning process (by taking into account the segmentations performed by the method) and (*iii*) use of parameters of high level (for instance shape descriptors). Points (*i*) and (*ii*) will require to develop solutions to reinject the evaluation of the segmentations in the learning/segmentation process, while point (*iii*) will require to develop solutions to compute (or at least approximate) complex attributes with a satisfactory algorithmic cost.

References

1. B. Bouraoui, C. Ronse, J. Baruthio, N. Passat, and P. Germain. 3D segmentation of coronary arteries based on advanced Mathematical Morphology techniques. *Computerized Medical Imaging and Graphics*, In press (doi: 10.1016/j.compmedimag.2010.01.001).
2. E. J. Breen and R. Jones. Attribute openings, thinnings, and granulometries. *Computer Vision and Image Understanding*, 64(3):377–389, 1996.
3. B. Caldairou, B. Naegel, and N. Passat. Segmentation of complex images based on component-trees: Methodological tools. In *International Symposium on Mathematical Morphology - ISMM'09, 9th International Symposium, Proceedings*, volume 5720 of *Lecture Notes in Computer Science*, pages 171–180. Springer, 2009.

4. L. Chen, M. W. Berry, and W. W. Hargrove. Using dendronal signatures for feature extraction and retrieval. *International Journal of Imaging Systems and Technology*, 11(4):243–253, 2000.
5. H. E. Cline, D. R. Thedens, C. H. Meyer, D. G. Nishimura, T. K. Foo, and S. Ludke. Combined connectivity and a gray-level morphological filter in magnetic resonance coronary angiography. *Magnetic Resonance in Medicine*, 43(6):892–895, 2000.
6. J. Cousty, L. Najman, M. Couprie, S. Clément-Guinaudeau, T. Goissen, and J. Garot. Segmentation of 4D cardiac MRI: Automated method based on spatio-temporal watershed cuts. *Image and Vision Computing*, In press (doi: 10.1016/j.imavis.2010.01.001).
7. G. Gerig, T. Koller, G. Székely, C. Brechbühler, and O. Kübler. Symbolic description of 3-D structures applied to cerebral vessel tree obtained from MR angiography volume data. In *Information Processing in Medical Imaging - IPMI'93, Proceedings*, volume 687 of *Lecture Notes in Computer Science*, pages 94–111. Springer, 1993.
8. M. K. Hu. Visual pattern recognition by moment invariants. *IRE Transactions on Information Theory*, 8(2):179 –187, 1962.
9. R. Jones. Connected filtering and segmentation using component trees. *Computer Vision and Image Understanding*, 75(3):215–228, 1999.
10. D. Lesage, E. D. Angelini, I. Bloch, and G. Funka-Lea. A review of 3D vessel lumen segmentation techniques: Models, features and extraction schemes. *Medical Image Analysis*, 13(6):819–845, 2009.
11. B. Naegel, N. Passat, N. Boch, and M. Kocher. Segmentation using vector-attribute filters: methodology and application to dermatological imaging. In *International Symposium on Mathematical Morphology - ISMM 2007, Proceedings*, volume 1, pages 239–250. INPE, 2007.
12. B. Naegel, N. Passat, and C. Ronse. Grey-level hit-or-miss transforms - Part II: Application to angiographic image processing. *Pattern Recognition*, 40(2):648–658, 2007.
13. L. Najman and M. Couprie. Building the component tree in quasi-linear time. *IEEE Transactions on Image Processing*, 15(11):3531–3539, 2006.
14. G. K. Ouzounis and M. H. F. Wilkinson. Mask-based second-generation connectivity and attribute filters. *IEEE Transactions on Pattern Analysis and Machine Intelligence*, 29(6):990–1004, 2007.
15. P. Salembier, A. Oliveras, and L. Garrido. Anti-extensive connected operators for image and sequence processing. *IEEE Transactions on Image Processing*, 7(4):555–570, 1998.
16. O. Tankyevych, H. Talbot, P. Dokládal, and N. Passat. Direction-adaptive grey-level morphology. Application to 3D vascular brain imaging. In *International Conference on Image Processing - ICIP'09, Proceedings*, pages 2261–2264. IEEE Signal Processing Society, 2009.
17. E. R. Urbach, N. J. Boersma, and M. H. F. Wilkinson. Vector attribute filters. In *International Symposium on Mathematical Morphology - ISMM 2005, Proceedings*, volume 30 of *Computational Imaging and Vision*, pages 95–104. Springer SBM, 2005.
18. E. R. Urbach, J. B. T. M. Roerdink, and M. H. F. Wilkinson. Connected shape-size pattern spectra for rotation and scale-invariant classification of gray-scale images. *IEEE Transactions on Pattern Analysis and Machine Intelligence*, 29(2):272–285, 2007.
19. E. R. Urbach and M. H. F. Wilkinson. Shape-only granulometries and gray-scale shape filters. In *International Symposium on Mathematical Morphology - ISMM 2002, Proceedings*, pages 305–314. CSIRO Publishing, 2002.
20. V. Vapnik. *Statistical Learning Theory*. Wiley-Interscience, New York, 1998.
21. M. H. F. Wilkinson and M. A. Westenberg. Shape preserving filament enhancement filtering. In *Medical Image Computing and Computer-Assisted Intervention - MICCAI 2001, Proceedings*, volume 2208 of *Lecture Notes in Computer Science*, pages 770–777. Springer, 2001.